THE SUNLIT LUNAR SURFACE

II. *A Study of Far Infrared Brightness Temperatures*

J. M. SAARI†, R. W. SHORTHILL, and D. F. WINTER*
Boeing Scientific Research Laboratories, Seattle, Washington, U.S.A.

(Received 23 November, 1971)

Abstract. Directional infrared emission from the sunlit lunar surface is determined for the thermal meridian and as a function of observer elevation and azimuth angles at three Sun elevation angles. A study of selected mare sites at full Moon suggests that brightness temperatures are relatively insensitive to changes in certain surface parameters, such as the photometric function, emissivity, and thermophysical properties of the soil. The observed deviations from predictions for an 'average' surface can be accounted for by changes in surface roughness.

1. Introduction

Because of the highly insulating properties of the general lunar surface, conduction into the sunlit surface will be small compared to the absorption of solar radiation and emission at far infrared wavelengths. Consequently, if the surface were a smooth gray-body Lambertian emitter, as is assumed for many theoretical thermophysical models, the brightness temperature T_L of the surface would be given by

$$T_L = T_s \cos^{1/4} \theta , \tag{1}$$

provided the solar zenith angle θ is not too large and where T_s is the temperature the surface would attain if the Sun were in the zenith. If the emissivity ε and bolometric albedo A_b are known, then T_s can be calculated from

$$T_s = [S(1 - A_b)/\varepsilon\sigma]^{1/4} , \tag{2}$$

where S is the solar insolation and σ is the Stefan-Boltzmann constant. If ε is assumed to be unity, the calculated T_L, designated hereafter as the Lambertian temperature, is the temperature of a black body radiating the same power that is absorbed from the Sun.

It is well known that systematic discrepancies exist between measurements of brightness temperatures of the sunlit surface and those predicted from a smooth black-body model. The purpose of this paper is to present a definitive description of the brightness temperature measurements of the sunlit surface and to estimate the extent to which various properties of the surface can account for the observed effects.

2. Measurements of Directional Effects

In Part I (Saari and Shorthill, 1972) it was determined that the brightness temperature

* Department of Oceanography, University of Washington, Seattle, Washington, U.S.A.
† Deceased 12 January, 1971.

The Moon **5** (1972) 179–199.

distribution observed over the full Moon could be represented by a function linear in $\cos\theta$. This description of the directional emission of the surface applies to the special case where the vectors to the Sun and observer coincide.

The search for a more general description of the directional emission from the sunlit surface began with a study of brightness temperature T_b as a function of Sun elevation angle χ for several locations along the lunar equator. The data were extracted from isothermal maps made at a number of phase angles as reported by Saari and Shorthill (1967a). By way of example, Figure 1 shows results corresponding to the

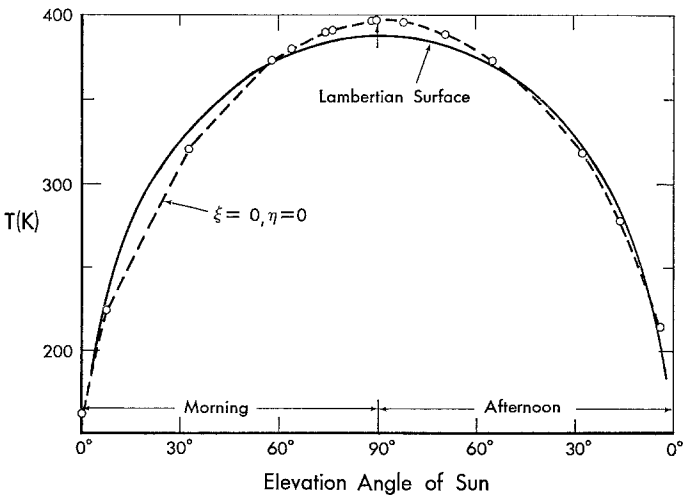

Fig. 1. Sunlit brightness temperatures for the center of the Moon. In this figure and in Figures 2 and 3 the vertical arrow indicates data from the full Moon and the solid line is the calculated Lambertian temperature.

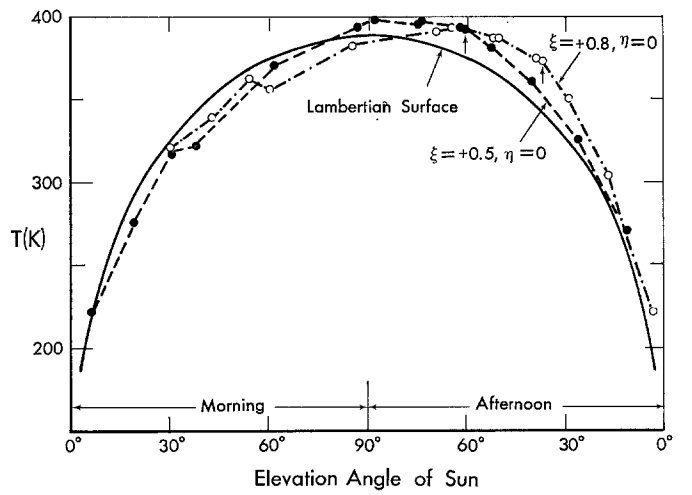

Fig. 2. Sunlit brightness temperatures on the equator for two locations, ξ=0.8 and 0.5.

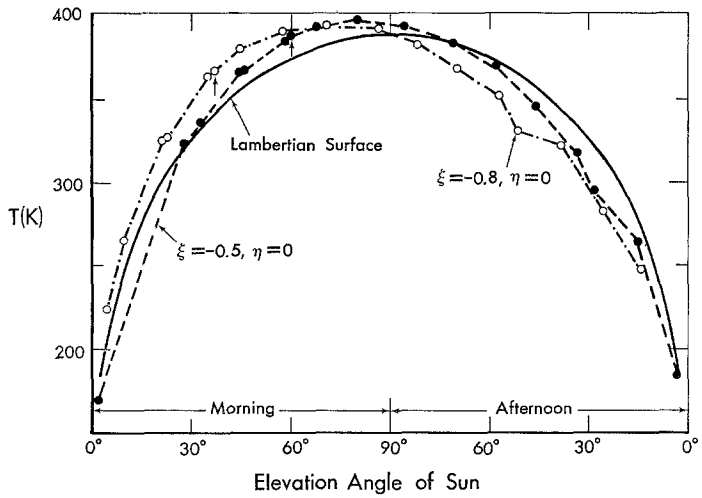

Fig. 3. Sunlit brightness temperatures on the equator for two locations: $\xi = -0.8$ and -0.5.

center of the lunar disk. Plotted in the same figure is the Lambertian temperature, as calculated from Equation (1), using a bolometric albedo appropriate to the center of the Moon. It can be seen from the figure that, when the sun elevation angle is greater than about 50°, the brightness temperature is higher than the Lambertian temperature. The same is true at low Sun angles, both for the morning and afternoon data. Similar plots for $\xi = \pm 0.5$ and ± 0.8 are shown in Figures 2 and 3. In all cases, the measurements suggest that T_b exceeds T_L when the surface is observed from the general direction of the Sun. It is evident from these curves that a certain amount of care must be exercised when comparing isotherms with theoretical predictions of smooth thermophysical models, since the sunlit surface exhibits directionality in the infrared.

The data were characterized by a fair amount of scatter, as is apparent in Figures 1, 2, and 3. A consideration of the discrepancies suggested that the scatter was due primarily to the fact that scans were made at different librations. Accordingly, we decided to undertake a more systematic study of directional emission from the thermal meridian, which is defined as the great circle passing through the subsolar point and the topcentric center of the lunar disk (Montgomery *et al.*, 1966). With this definition, the normal to a surface element on the thermal meridian is coplanar with vectors from the element to the Sun and to the observer. It is useful to express the directionality of emission in terms of the ratio of the observed brightness temperature to the calculated Lambertian temperature. The ratio T_b/T_L was termed a directional factor, or D-factor,* by Saari and Shorthill (1967b).

* There is no compelling reason for preferring the D-factor as a measure of directionality. However, we specifically decided against describing the phenomenon in terms of directional emissivity, which is defined as the radiance in a certain direction compared with that of a black-body at the same

As a special case of the data along the thermal meridian, temperatures at the limb (zero observer elevation angle) were studied as a function of phase angle. The procedure involved extrapolation of signal values along the thermal meridian to the position of the sunlit limb. The resulting values of directional factors D are plotted against phase angle in Figure 4. Clearly, the largest values of D are observed at the smallest values of the phase angle. At a phase angle of 90°, when the subsolar point is on the

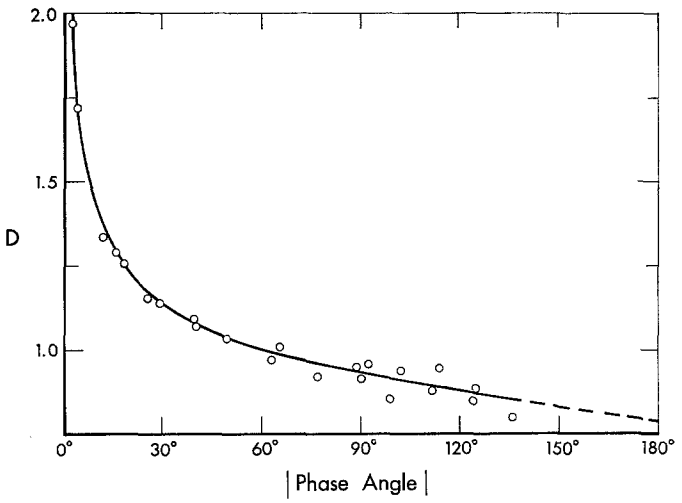

Fig. 4. Limb values of the directional factor D for the thermal meridian as a function of phase angle. The dashed portion of the curve is extrapolated.

limb, the curve through the data was constrained to pass through a value of 0.933, as inferred from the data of Sinton (1962) on the variation of planetary heat of the subsolar point with phase.

We next determined the directional factors for Sun elevation angles of 10°, 20°, ..., 80° as a function of observer elevation angle. To do so, temperatures were read from the isothermal contours at the measured phases along the thermal meridian at 10° intervals from the subsolar point. Directional factors were calculated for each point, taking into account the local albedo and the Sun–Moon distance. The results are shown in Figures 5 through 12 for each of the Sun elevation angles. In these figures, the observer elevation angle ζ is less than 90° when the Sun and observer vectors are

---

temperature. Implicit in this definition is the assumption that all elements of the surface are at the same temperature. However, in the case of telescopic measurements of the illuminated Moon, the field of view includes local surface elements having different inclinations with respect to the Sun, so that actually a heterogeneous temperature field is observed. Because this requires a non-traditional interpretation of directional emissivity, we decided to use the directional factor instead. We do not mean to imply by this choice that the surface does not possess directional emissivity in accordance with the above definition.

on the same side of the surface normal; i.e., the Sun is behind the observer. For values of ζ greater than 90°, the observer faces the Sun. At observer elevation angles of 0° and 180°, the smooth curves through the data were constrained to pass through the limb values of D, as read from Figure 4. Moreover, those points where the observer and Sun elevation angles are equal correspond to data on the full Moon. For these points a directional factor was calculated from the results in Part I: namely,

$$D = 1.032\,(0.8093 + 0.1807\cos\theta)/\cos^{1/4}\theta, \tag{3}$$

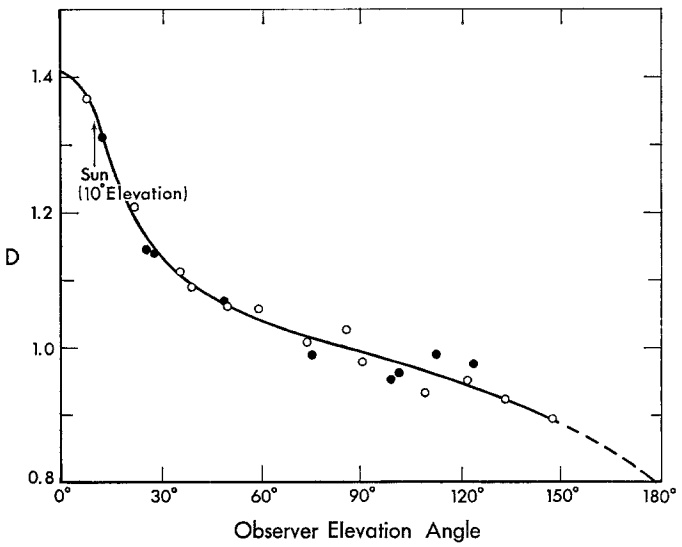

Fig. 5. Directional factor D on the thermal meridian for a Sun elevation angle of 10°. In this figure and Figures 6–12 the open circles represent afternoon data and the filled circles morning data. In Figures 5–7 the dashed portion of the curve is drawn to a value at right margin obtained from the extrapolated portion of the curve in Figure 4.

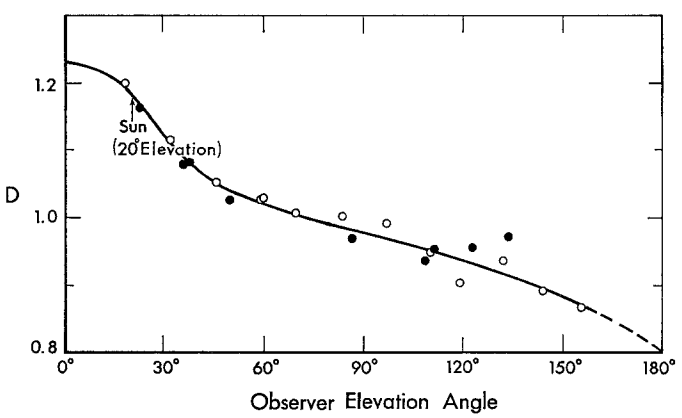

Fig. 6. Directional factor D on the thermal meridian for a Sun elevation angle of 20°.

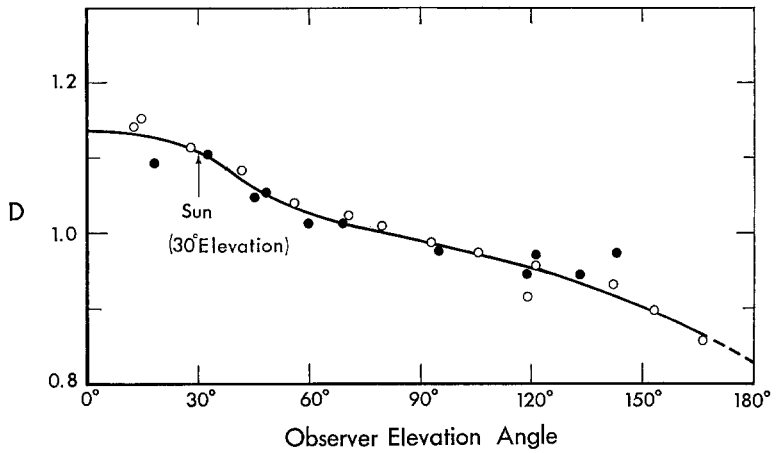

Fig. 7. Directional factor D on the thermal meridian for a Sun elevation angle of 30°.

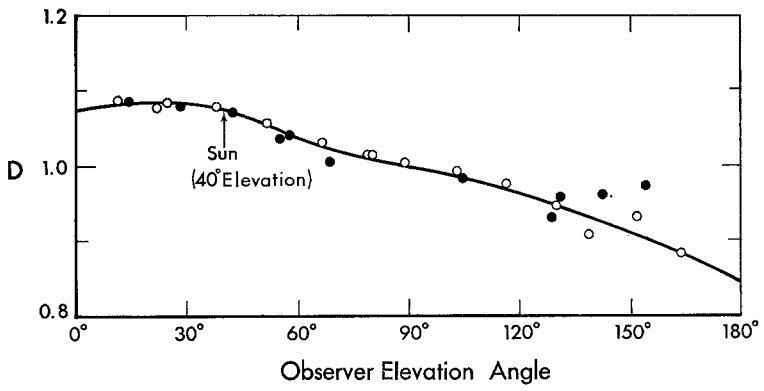

Fig. 8. Directional factor D on the thermal meridian for a Sun elevation angle of 40°.

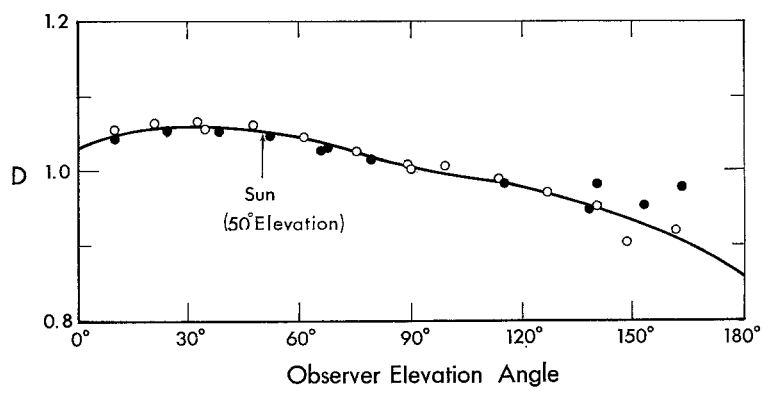

Fig. 9. Directional factor D on the thermal meridian for a Sun elevation angle of 50°.

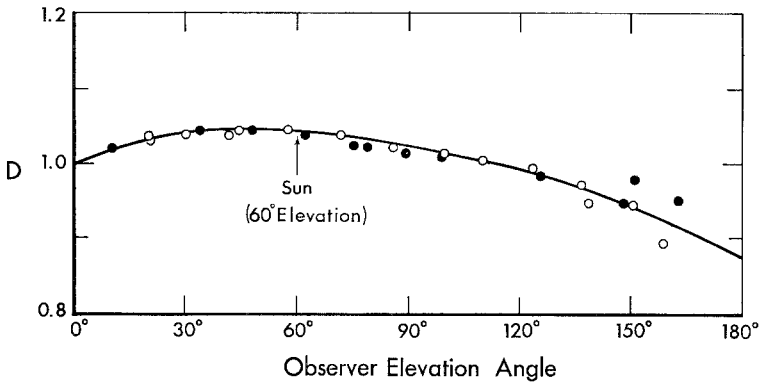

Fig. 10. Directional factor D on the thermal meridian for a Sun elevation angle of 60°.

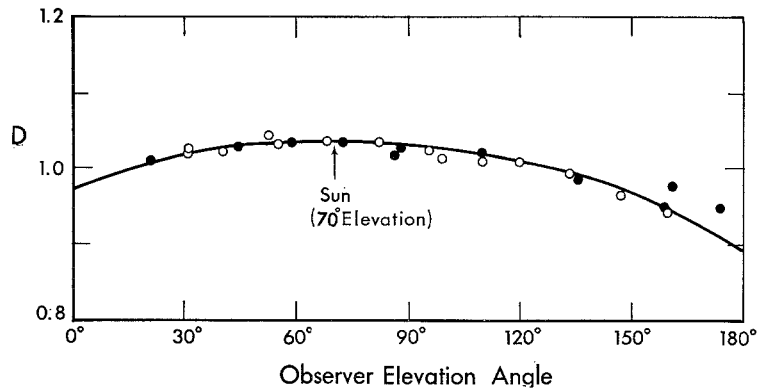

Fig. 11. Directional factor D on the thermal meridian for a Sun elevation angle of 70°.

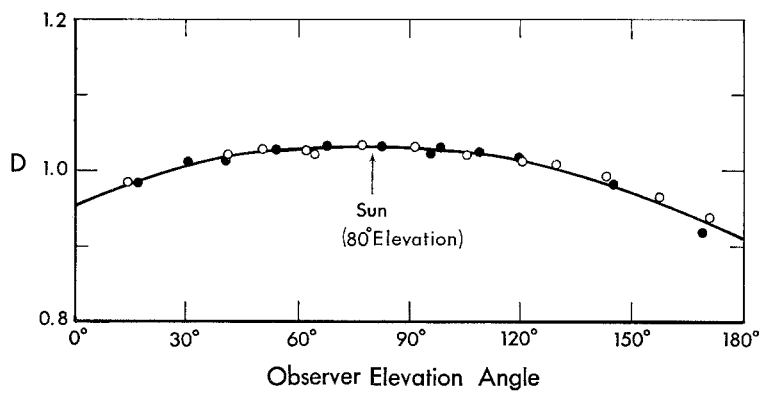

Fig. 12. Directional factor D on the thermal meridian for a Sun elevation angle of 80°.

where the factor 1.032 is the directional factor of the subsolar point at zero phase, $\theta=\pi/2-\zeta$, and the expression with the parentheses is the linear cosine law. The smooth curves in Figures 5 through 12 were accordingly constrained to pass through these calculated values, as well. The departure of D from unity is most pronounced at low Sun angles.

All of the data for different Sun angles can be summarized in a contour chart of D as shown in Figure 13, where the abscissa is the observer elevation angle and the

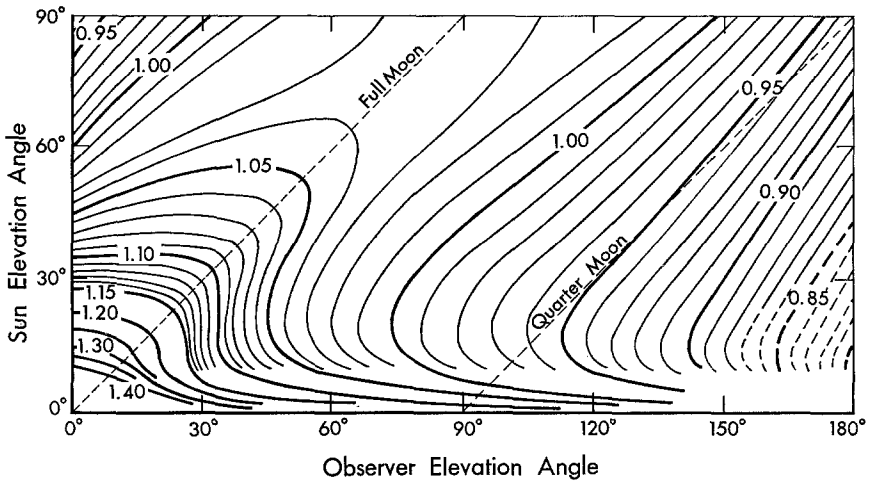

Fig. 13. Smoothed contour plot of directional factor D for the thermal meridian as a function of Sun and observer elevation angles. Dashed lines indicate extrapolated data.

ordinate the Sun elevation angle. In this plot, thermal meridian data for a scan at a particular phase angle lie along lines inclined at 45° to the axis of the plot. For example, the dotted lines shown in the figure correspond to full- and quarter-Moon. The data along the upper boundary of the figure correspond to Sinton's measurements of the subsolar point variation with phase. A certain amount of smoothing has been applied to the contours in the upper right and left corners of the figure. The contours for Sun angles less than 10° were determined from data in mare from five scans with phase angles ranging from about +40° to +135°. These contours suggest that the directional factor increases markedly as the Sun approaches grazing incidence over a wide range of observer angles.

Contour plots similar to Figure 13 have been published previously (Saari and Shorthill, 1967b; Winter and Krupp, 1971). However, the present diagram is intended to supplant the earlier versions, inasmuch as it is more complete (including data from the limb and at low Sun angles) and more accurate (being additionally constrained to agree with the linear cosine law for the full Moon). It is useful for comparison with theoretical models of surface roughness since it requires calculations only along the lunar equator.

The directional characteristics summarized in Figure 13 pertain only to the thermal meridian. More generally, of course, directionality will also depend on the azimuth angle of the observer. The nature of this dependence was ascertained from a separate study of the temperature data corresponding to Sun elevation angles of 10°, 30°, and 60°. At each phase, a given Sun elevation angle corresponds to a 'latitude' circle in a system in which the subsolar point is a pole. Brightness temperatures were read from the appropriate latitudes, taking data at 10° intervals in 'longitude'. D-factors were then calculated after making corrections for the albedo and Sun–Moon distance. For each point the observer azimuth angle ϕ (taken to be zero when the projections of the Sun and observer vectors on the surface coincided) and elevation angle ζ were calculated. In this study, ζ ranges from 0° to 90°. A least squares spherical harmonic fit to the data was made for each Sun elevation angle using the following expression

$$D = D_0 + \sum_{i=i}^{4} \sum_{j=0}^{i} [J_{ij} \cos(j\lambda) + J'_{ij} \sin(j\lambda)] P_i^j(X), \tag{4}$$

where $X = \sin\beta$, J_{ij} and J'_{ij} are constants and $P_i^j(X)$ is an associated Legendre polynomial. The parameters β and λ are related to the angles ϕ and ζ by means of the relations

$$\sin\beta = -\cos\phi\cos\zeta,$$
$$\sin\lambda = \frac{\cos\zeta - \sin\beta\cos\phi}{\cos\beta\sin\phi}, \tag{5}$$

TABLE I

Coefficients for spherical harmonic fit to directional factors[a]

	Sun elevation angle		
	10°	30°	60°
D_0	0.9915	0.9944	0.9946
J_{10}	−0.1604	−0.1168	−0.4693(−1)
J_{20}	0.1567(−1)	0.3377(−2)	−0.1436(−1)
J_{30}	−0.1081	−0.2596(−1)	−0.2504(−2)
J_{40}	0.8890(−2)	−0.6777(−2)	−0.6000(−2)
J'_{11}	−0.1019(−6)	0.1160(−8)	−0.1443(−9)
J'_{21}	−0.3455(−7)	0.4353(−9)	0.5316(−9)
J'_{31}	−0.1266(−8)	0.3297(−9)	−0.6885(−9)
J'_{41}	0.3723(−7)	−0.1782(−10)	0.6238(−10)
J_{22}	0.1068(−2)	0.1263(−2)	0.1028(−1)
J_{32}	0.3074(−2)	0.2253(−2)	0.2125(−4)
J_{42}	0.1061(−2)	0.1492(−3)	0.3272(−3)
J'_{33}	0.5602(−8)	−0.7602(−11)	−0.4417(−10)
J'_{43}	0.4240(−9)	−0.8132(−11)	−0.2403(−10)
J'_{44}	0.7914(−5)	−0.1359(−4)	−0.8018(−4)

[a] The numbers in parenthesis indicate the power of ten by which the entry should be multiplied.

and

$$\cos\lambda = \frac{\sin\zeta}{\cos\beta}.$$

The spherical harmonic fit imposes a symmetry in ζ, i.e. $D(\zeta, \phi) = D(-\zeta, \phi)$. Moreover, with the requirement that the results be symmetrical with respect to ϕ, i.e. $D(\zeta, \phi) = D(\zeta, -\phi)$, only certain J_{ij}'s and J'_{ij}'s are used. The values of these constants are given in Table I.

Contours of the resulting directional factors are shown in Figures 14, 15, and 16. In each of these plots the vertical line ($\phi = 0°$ and 180°) corresponds to the thermal meridian, so that data along this line should correspond to the results displayed in Figures 5, 7, and 10. However, a certain amount of discrepancy is to be noted (e.g., the shallow maximum in Figure 14 contradicts the data in Figure 5) which arises for two reasons. First, the spherical harmonic fit is based on a different set of experimental data, and secondly, the symmetry in ζ implies that $(\partial D/\partial\zeta)$ is zero at $\zeta = 0$. This constraint is a mathematical artifice introduced by the fitting process and is not indicated by the data in Figures 5 through 12. Accordingly, the spherical harmonic fits in Figures 14, 15, and 16 indicate only the general nature of the azimuthal dependence.

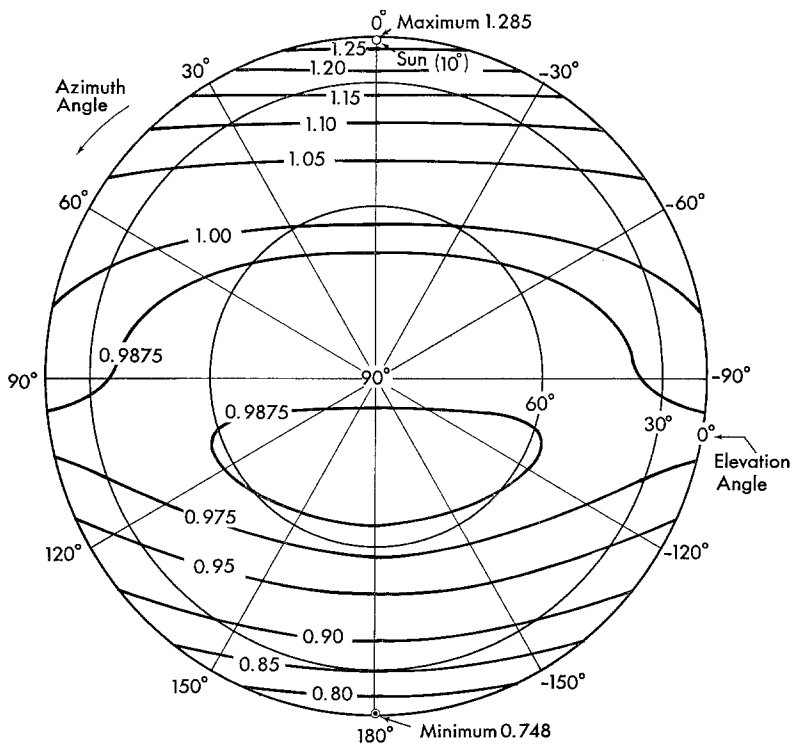

Fig. 14. Dependence of directional factor D on azimuth and elevation angles of the observer obtained from a spherical harmonic fit to data for a Sun elevation angle of 10°.

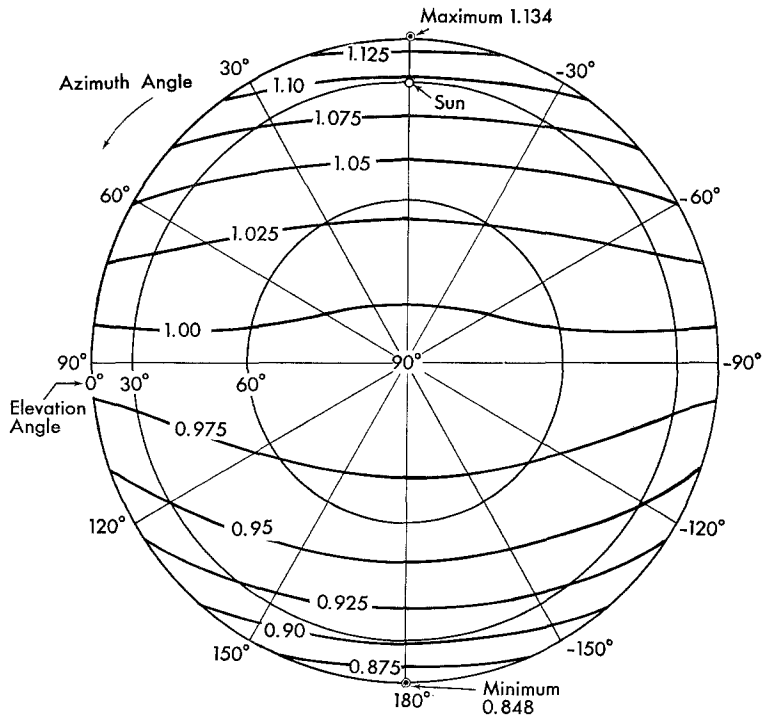

Fig. 15. Dependence of directional factor D on azimuth and elevation angles of the observer obtained from a spherical harmonic fit to data for a Sun elevation angle of 30°.

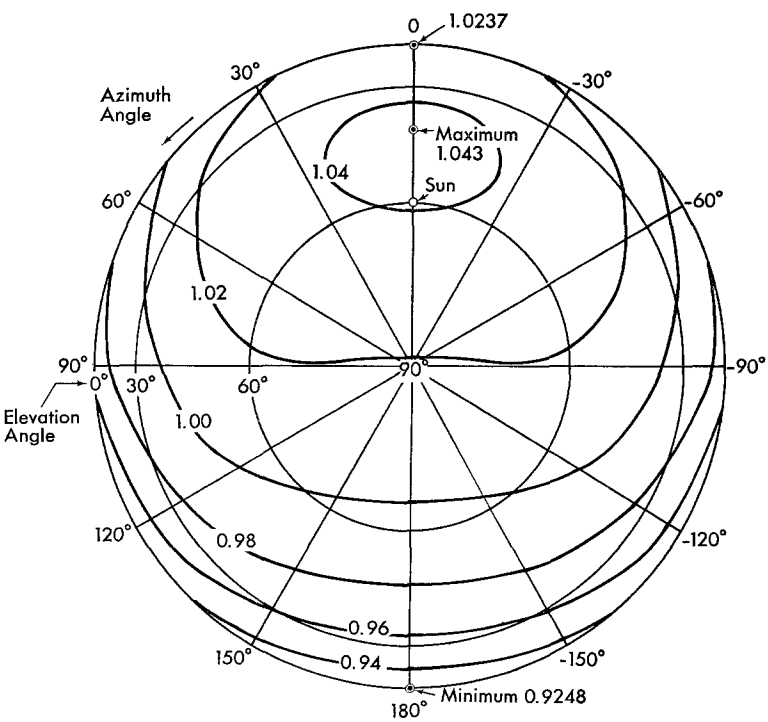

Fig. 16. Dependence of directional factor D on azimuth and elevation angles of the observer obtained from a spherical harmonic fit to data for a Sun elevation angle of 60°.

3. Parameters Affecting Brightness Temperatures

The effects of albedo and directional emission on measured brightness temperatures of the sunlit lunar surface presented in Part I and the previous section should be considered to apply to an 'average' surface since the determinations were made with data for points scattered over the disk. However, localized differences in the photometric function and surface roughness could affect the measurements, as well as other factors such as the thermophysical properties and emissivity. In this section quantitative studies of the influence of these parameters are compared with observed deviations from brightness temperatures predicted for the 'average' surface.

3.1. Photometric function

First, we consider the effect of changes in the photometric function, or more specifically the sharpness of the backscattering of the incident sunlight. This property is conveniently measured by the magnitude of a compaction parameter H which is related to the porosity of the top surface layer, with lower values of H implying sharper backscattering. The parameter H was formulated by Hapke (1966) in his description of the lunar photometric function. More recently, Shorthill *et al.* (1969) studied the photometry of 300 sites through a lunation, fitting each observed phase curve to Hapke's function by varying the photometric parameters. In the course of this study, it was found that H varied from 0.1 to more than 1.1. Since this range is so large, it is reasonable to expect that regional changes in H should produce corresponding changes in the measured brightness temperature. In order to investigate this possibility, 21 sites in different maria encompassing a wide range of H were selected

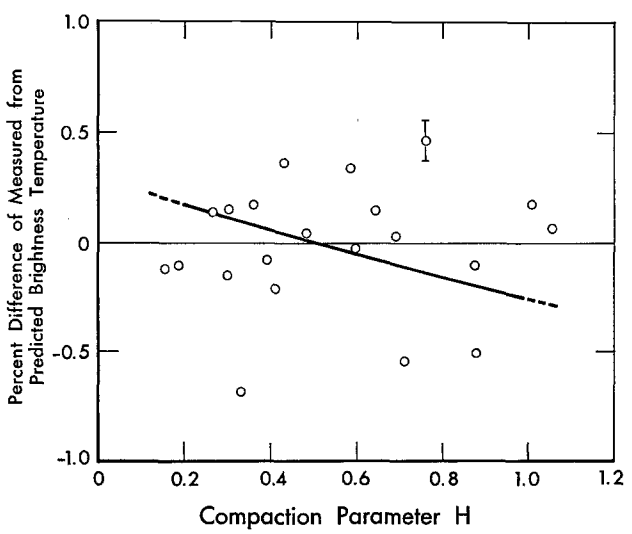

Fig. 17. Deviations between measured and predicted brightness temperatures for mare sites on the full Moon as a function of compaction parameter H. Expected variation shown by solid line.

from the 300 photometric sites. To assess the effect on brightness temperature, data from the nearest full Moon were utilized. For each site, a predicted brightness temperature for an 'average' surface was calculated using the albedo correction and linear cosine law determined in Part I. The resulting difference of the measured brightness temperature at the site from the predicted value was then used as a measure of the departure of the local from the 'average' surface. The results shown in Figure 17 do not indicate a systematic variation with H.

One might inquire as to what brightness temperature variation might be expected to accompany changes in H. To answer this question, the total integrated light reflected from a surface element is required. Since Hapke did not perform this integration, we utilized the results of Burkhard and Ashby (1967). These workers used a somewhat modified version of Hapke's function to calculate the total integrated energy reflected from the surface as a function of H and elevation angle of the Sun. For purposes of illustration, we used their results for an elevation angle of 60° (corresponding to points halfway to the limb) and an albedo equal to the average of the 21 sites. The resulting change in temperature with H was referenced to the temperature calculated for $H=0.5$. The predicted curve is shown as a solid line in Figure 17; similar calculations for the center of the Moon yielded essentially the same curve.

These results suggest that some other effect is masking the variation expected from changes in the compaction parameter H. One obvious possibility is that experimental error contributes to the scatter of the data. Therefore, an error analysis was performed for a sample point, taking into account errors arising from (1) voltage fluctuations in the infrared signal, (2) interpolation between isotherms in reading brightness temperature, and (3) position inaccuracies in the calculation of normalized temperature from the linear cosine law. The resulting error bar is shown Figure 17. If we are correct in interpreting this error bar as being fairly representative, then the observed deviations are significantly larger than the expected error. It is also possible that the linear cosine law may not adequately depict the average brightness temperature. However, if this is so, we should expect some systematic variation in temperature discrepancy over the disk. However, a plot of the deviations in selenographic coordinates did not reveal such a dependence on position. These considerations suggest that the deviations are real. The rms deviation of the 21 points from the solid line giving the compaction parameter variation is 0.32%. Although this corresponds to about three times the estimated experimental error, the deviations are actually rather small, at least for the selected mare sites. It is not known what deviations might be found for sites in the uplands. Such sites were deliberately excluded from this study so as to avoid introducing additional factors, such as the effect of local slope on temperature.

3.2. Emissivity

There is also a possibility that variations in emissivity could give rise to the observed deviations. In this connection, Murcray *et al.* (1970), using a balloon-borne infrared spectrometer, have measured the emissivity of six regions on the Moon in the far infrared. Their results were characterized by a peak (which they set equal to unity)

in the region of 8–8.5 μ, followed by a more or less flat plateau extending from about 10 μ to beyond 13 μ. The data also suggested a certain amount of regional variation in the level of the plateau. At the mean wavelength of our infrared detector (11 μ), the values ranged from 0.882 to 0.915. In order to elucidate the manner in which emissivity variations can change brightness temperatures measured by our detector, consider a reference area at a kinetic temperature T_r with emissivity $\varepsilon_r(\lambda)$. The output signal of a narrow-band detector operating at 11 μ looking at this surface will be proportional to the product of its response function (Planck's function at 11 μ) and $\varepsilon_r(11\ \mu)$. By definition, the brightness temperature $T_{r,b}$ provides the same output signal with an assumed unit emissivity, so we can write

$$\frac{\varepsilon_r(11\mu)}{\exp(T_d/T_r)-1} = \frac{1}{\exp(T_d/T_{r,b})-1}, \tag{6}$$

where the characteristic temperature T_d is 1308 K for an 11 μ detector. This expression indicates that a considerable discrepancy may exist between brightness and kinetic temperature. For instance, if $T_{r,b}=390$ K and $\varepsilon_r(11\ \mu)=0.9$, then $T_r=402.2$ K. Consider next another area (m) with emissivity $\varepsilon_m(\lambda)$ which is identical with the reference area to the extent that it radiates the same power as the reference area:

$$\int_0^\infty \varepsilon_r(\lambda)\, B(\lambda, T_r)\, \mathrm{d}\lambda = \int_0^\infty \varepsilon_m(\lambda)\, B(\lambda, T_m)\, \mathrm{d}\lambda, \tag{7}$$

where $B(\lambda, T)$ is Planck's function and T_m is the kinetic temperature of the area (m). If ε_r, T_r, and ε_m are given, this expression makes it possible to determine T_m. Then, with an expression of the form of Equation (4), the brightness temperature $T_{m,b}$ can be calculated. The difference between $T_{m,b}$ and $T_{r,b}$ is due to the differing emissivities ε_r and ε_m of the two areas.

With reference to the data for the 21 mare sites under consideration, the following procedure was used to estimate the changes in emissivity necessary to account for the observed deviations. For each site we have a measured brightness temperature $T_{m,b}$ and a predicted temperature $T_{r,b}$. The latter was calculated using the per cent deviation from the curve determined in Figure 17 for the change to be expected with variations in the compaction parameter H. Therefore, $T_{r,b}$ was determined taking into account local albedo, directional characteristics, and the compaction parameter. Next, for the purpose of this calculation, the balloon-borne emissivity measurements were idealized by setting ε equal to unity for $7.7\ \mu<\lambda<8.7\ \mu$ and to an appropriate constant value (ε_r and ε_m) for all other wavelengths. The choice of ε_r for the reference surface should represent in some way an average value for the disk. Due to the lack of such information, and in view of the rather idealized assumptions made regarding the functional form of $\varepsilon(\lambda)$, we assumed $\varepsilon_r=0.890$, the value obtained by the balloon-borne measurements in the region of the subsolar point at 11 μ. Admittedly, the choice of ε_r is somewhat arbitrary. However, we are primarily interested in changes in emissivity necessary to explain the observed brightness temperature deviations. In the present

context, this choice for ε_r may have a certain justification since the subsolar point was used as the calibration point for the determination of brightness temperatures over the rest of the disk. With the assumed value of ε_r and a given value of $T_{r,b}$, a value of ε_m could be calculated which accounted for the measured $T_{m,b}$. The results for the 21 points are shown in Figure 18. Since the results depend to some extent on $T_{r,b}$, the curves in the figure illustrate expected variations for two values of 370 and 400 K.

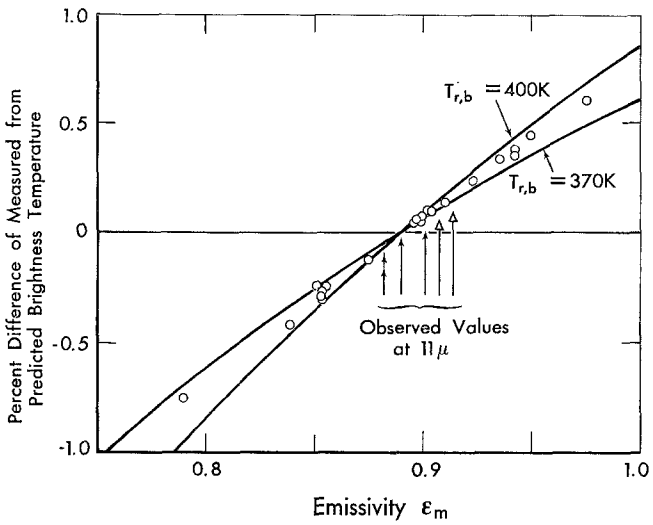

Fig. 18. Variation in emissivity necessary to account for full Moon brightness temperature deviations. It was assumed the predicted temperature $T_{r,b}$ in each case was characterized by a surface with $\varepsilon_r = 0.89$. The vertical arrows correspond to observed values of emissivity at 11 μ obtained with a balloon-borne spectrometer by Murcray *et al.* (1970).

For the purposes of comparison, values of emissivity measured at 11 μ by the balloon-borne experiment are also indicated; two mare areas, Serenitatis and Imbrium, are identified by the open arrows. It can be seen that the range of emissivity values required to reproduce the observed brightness temperature deviations is considerably greater than the range observed by the balloon-borne spectrometer.

It should be noted that the balloon-borne spectrometer had a field of view of 3′ arc, compared with our value of 10″ arc, thereby corresponding to an area on the Moon larger by about a factor of 300. One cannot, therefore, discount the possibility that the larger field of view effectively averaged variations which occurred over a smaller scale comparable to our field of view. Of use in this connection are the observations reported by Goetz (1968) who performed Earth-based differential emissivity measurements for 22 areas on the Moon at a resolution of 20″–40″ arc. Except for the possibility of several per cent lower emissivity in the region 8.2–9.0 μ for Plato and Mare Humorum, no significant deviations greater than 0.5–1.0% were found. It should be noted, however, that spectral features less than about 2 μ in width would be suppressed considerably because of the particular technique used in his analysis. In any event, if

the balloon-borne emissivity measurements can be considered to represent variations over the lunar surface, then corresponding variations in brightness temperatures would amount to only about $\pm 0.1\%$ on the basis of the simplified form of $\varepsilon(\lambda)$ used in the estimation.

Measurements at higher resolution and over a wider range of wavelengths would be needed to define the relationship between brightness temperatures and emissivity with greater precision. Actually, the impetus for refined measurements lie in the diagnostic possibilities as discussed by Conel (1969) and (with respect to the balloon-borne measurements) by Salisbury *et al.* (1970). Finally, the discrepancy between the kinetic temperature and the brightness temperature caused by the departure of the emissivity from unity, discussed by Burns and Lyon (1964), should be taken into account in theoretical thermophysical models when comparisons are to be made with the measured thermal response of specific areas.

3.3. THERMOPHYSICAL PROPERTIES

Next, we consider the possibility that variations of surface thermophysical properties may produce the observed deviations of brightness temperature. As is well known, the thermophysical properties of the lunar surface are best revealed under eclipse or nighttime conditions. During illumination, the conduction into the surface is small compared to the solar input and radiative output because of the generally excellent insulating properties of the surface. As a consequence, sunlit surface temperatures should be relatively insensitive to modest changes in thermophysical properties. With respect to the mare data under consideration here, a definitive assessment of the effect of parameter variations would entail a search for satisfactory thermophysical parameters for each site based on eclipse and lunation cooling data. The deviations during illumination from an 'average' surface could then be determined. Since this information is unavailable for the 21 sites, we shall consider instead one particular site which is located in Mare Humorum. Its measured brightness temperature was 0.76% less than the predicted value, taking into account the effects of albedo, directional emission, and compaction parameter. This was the largest deviation observed for the 21 sites. From infrared eclipse measurements (Saari and Shorthill, 1965), Mare Humorum was found to be thermally enhanced by about 10–12 K over its environs which was, along with parts of Oceanus Procellarum, the largest enhancement observed in the maria. If the enhancement is due to a general change in the thermophysical properties, it is reasonable to expect the temperature of the area to fall below that of the environs during the morning because of its greater thermal inertia. For the purpose of estimating an expected temperature difference, we utilize the constant thermophysical properties model of the lunar surface. While this model does not accurately depict both eclipse and lunation cooling, its simplicity recommends its use in the study of differential effects. In the present case, we utilize calculations based on values of the thermal parameter $\gamma = (k\varrho c)^{-1/2}$ equal to 800 and 500 (cal-cgs units). The former value gives results which agree with experiment for lunation cooling of the typical lunar surface (Winter and Saari, 1969) and is assumed to

describe the environs. Moreover, for the Mare Humorum site the $\gamma = 500$ curve is 11 K higher than the $\gamma = 800$ curve at local midnight and also reproduces the observed eclipse differential. Therefore, assuming these two values of γ apply to Mare Humorum and its environs, we calculated the corresponding percent difference in temperature during the daytime. The results are given in Figure 19 which shows the expected lag in the $\gamma = 500$ results as compared with the $\gamma = 800$ results. At that time during the

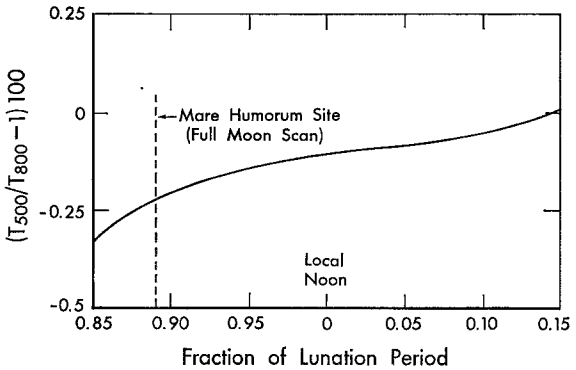

Fig. 19. Per cent difference in daytime temperatures for homogeneous thermophysical models with the thermal parameter $\gamma = (k\varrho c)^{-1/2}$ equal to 500 and 800 (cal-cgs units) for latitude of the Mare Humorum site.

lunation period which corresponds to the Mare Humorum site at full Moon, the $\gamma = 500$ curve is 0.23% below the $\gamma = 800$ curve. This is only one third of the observed deviation of 0.76%. Since this site departs thermophysically as much as any mare from the typical surface (on the basis of eclipse measurements), we may generalize our results to conclude that apparently only a part of the observed full Moon temperature deviation can be explained by differences in thermophysical properties.

3.4. Surface roughness

As a final possibility, we examine the influence of changes in surface roughness on measurements of brightness temperature. This topic has been discussed by a number of researchers whose work has recently been reviewed by Winter *et al.* (1972). It is shown in the cited review that models with different topographical idealizations, such as those of Bastin and Gough (1969) and Winter and Krupp (1971), yield qualitatively similar inferences regarding the effect of relief on directionality in the infrared. For the purposes of the present undertaking, we utilized the cratered-surface model proposed by Winter and Krupp (1971) which predicts contours of the directional factor in more or less general agreement with the experimental results of Figure 13. The model describes the cratered lunar surface by a composite of level regions and negative relief features consisting of 'sharp' (hemispherical) craters and 'subdued' craters with a depth-diameter ratio of 1:4. For given Sun and observer elevation

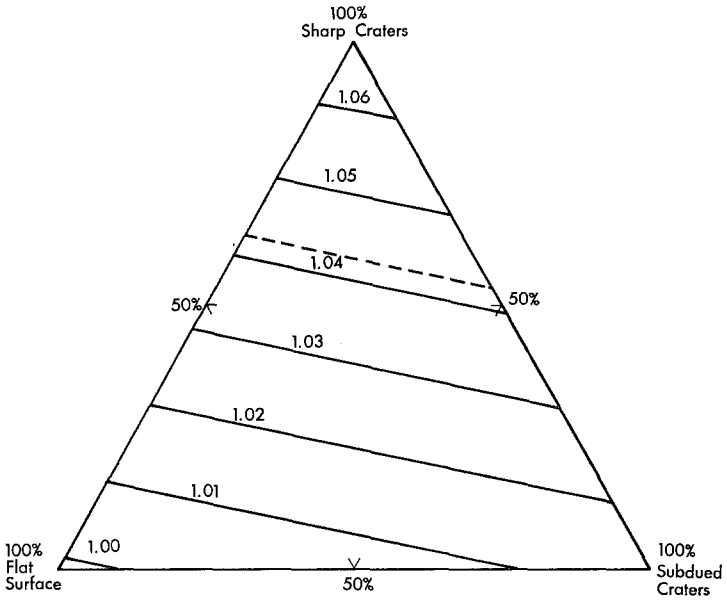

Fig. 20. Dependence of directional factor D on the relative coverage by three types of terrain according to the Winter-Krupp model. The Sun and observer elevation angles are coincident and equal to 60°. Dashed line indicates the experimental value of D calculated from the linear cosine law.

angles, calculations of the radiance associated with each terrain type lead to the determination of the apparent brightness temperature and directional factor for any combination of fractional areas of the three types of terrain. The results can be displayed on a triangular contour plot of D as shown in Figure 20 which is drawn for coincident Sun and observer elevation angles of 60°. The dashed line indicates the value obtained from the linear cosine law. Actually, as noted by Winter and Krupp (1971), the model generally yields values which are somewhat low at the high Sun elevation angles, perhaps because the soil itself exhibits directionality of emission not taken into account by the theory. This may account for the fact that similar triangular plots for other coincident elevation angles yield straight line loci for the observed directional factor (obtained from the linear cosine law) which do not intersect within the boundaries of the triangle. Thus, there is no unique combination of terrain types which will reproduce the observed directional factors over a range of Sun elevation angles on the full Moon. Notwithstanding this limitation, the model can be used to provide an estimate of the effect of changes in surface roughness. As can be seen from Figure 20, the directional factor is influenced most profoundly by changes in the fractional area F_c occupied by the sharp craters. Accordingly, calculations were made of changes in directional factor (hence brightness temperature) produced by changes in F_c. For this purpose, we used the average gradient in D along the line joining the 100% sharp craters point and the 50% flat surface – 50% subdued craters point for a range of elevation angles. The changes in brightness temperature produced by $\pm 10\%$

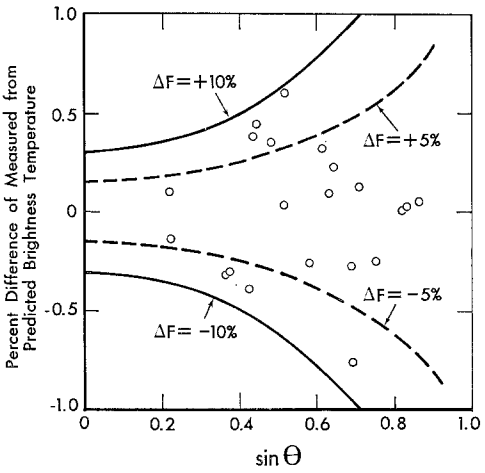

Fig. 21. Deviations between measured and predicted full Moon brightness temperatures as a function of normalized distance from the disk center. Curves show variation expected from indicated changes in coverage F_c by sharp craters according to the Winter-Krupp model.

and $\pm 5\%$ changes in F_c where then calculated and plotted as functions of the normalized distance from the disk center (Figure 21). Also shown are the measured values corresponding to the 21 mare sites. The curves for $\Delta F_c = \pm 10\%$ include all of the observed points; for $\Delta F_c = \pm 5\%$, thirteen of the observed points are included. This result indicates that relatively modest changes in the sharp crater coverage can account for observed temperature deviations.

4. Summary and Discussion

Improved values of the directional factor for the thermal meridian have been obtained from limb data and the linear cosine law for the full Moon. In particular, it was determined that the directional factor increased as the Sun elevation angle became small over a wide range of observer angles. Since most of the data used in this determination were taken near sunset, there is a possibility that the effect could be related to the effective thermal inertia of the surface, retarding the cooling in the late afternoon. To determine whether or not this is so, we studied data from three pairs of scans at approximately the same positive and negative phase angles near the terminator. The phases were chosen such that in all cases the terminator fell in smooth mare, thereby avoiding temperature changes due to variations in local slope over craters. The measured directional factors near the terminator are shown in Figure 22 for the six phase angles. In all cases, D increases as the Sun elevation angle decreases. Only in the plot for phase angles $+63.39°$ and $-65.48°$ does the afternoon data seem to be somewhat higher than the morning data. In any event, these results demonstrate that the directional factor undergoes an increase for low Sun angles in both the

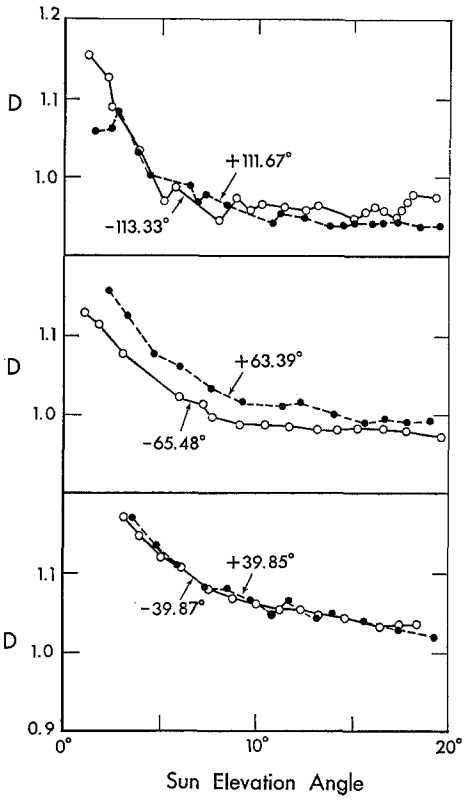

Fig. 22. Directional factor D on the thermal meridian obtained from scans of the lunar disk at the indicated phase angles. The data come from mare surfaces near the terminator.

morning and afternoon. The increase must, therefore, be associated with roughness of the surface rather than by thermal inertial effects near sunset. Consideration of the results obtained from the cratered surface model (Winter and Krupp, 1971) suggests that negative relief probably cannot explain the effect. It remains to be seen whether positive relief such as rocks on the surface, a likely alternative, can account for the observations.

We examined in some detail the parameters which can effect brightness temperatures of the illuminated lunar surface. The predominant cause of directionality of infrared emission is surface roughness; the deviations from a Lambertian surface can amount to many tens of percent at low Sun angles. The next important effect arises from changes in the local bolometric albedo which can produce deviations of several percent. For example, calculations show the average mare surface is two percent warmer than the average upland surface under the same illumination conditions. A study of a number of mare sites at full Moon showed that, after the above two effects are removed, the remaining deviations amount to only a few tenths of one percent. It was estimated that changes in the compaction parameter, emissivity, and

thermophysical parameters can result typically in deviations of several tenths of percent.

We conclude that remote observations of the sunlit lunar surface are mainly determined by the average surface roughness and local albedo and that the influence of other properties will be relatively small. Such considerations should be kept in mind in the interpretation of sunlit brightness temperatures obtained for other planetary surfaces such as Mercury.

Acknowledgement

The authors wish to express their appreciation to R. R. Green for calculating the spherical harmonic fits described in the text.

References

Bastin, J. A. and Gough, D. O.: 1969, *Icarus* **11**, 289.
Burkhard, D. G. and Ashby, N.: 1967, 'Study of Radiative Aspects of Lunar Materials', NASA Contract NAS8-20385, P.E.C. Research Associates, Inc., Boulder, Colorado
Burns, E. A. and Lyon, R. J. P.: 1964, *J. Geophys. Res.* **69**, 3771.
Conel, J. E.: 1969, *J. Geophys. Res.* **74**, 1614.
Goetz, A. F. H.: 1968, *J. Geophys. Res.* **73**, 1455.
Hapke, B.: 1966, *Astron. J.* **71**, 333.
Montgomery, C. G., Saari, J. M., Shorthill, R. W., and Six, N. F., Jr.: 1966, 'Directional Characteristics of Lunar Thermal Emission', Boeing Document D1-82-0568.
Murcray, F. H., Murcray, D. G., and Williams, W. J.: 1970, *J. Geophys. Res.* **75**, 2662.
Saari, J. M. and Shorthill, R. W.: 1965, *Nature* **205**, 964.
Saari, J. M. and Shorthill, R. W.: 1967a, 'Isothermal and Isophotic Atlas of the Moon', NASA Contractor Report CR-855.
Saari, J. M. and Shorthill, R. W.: 1967b, in *Physics of the Moon* (ed. by S. F. Singer), American Astronautical Society, Science and Technology Series **13**, 57.
Saari, J. M. and Shorthill, R. W.: 1972, *The Moon* **3**, 103.
Salisbury, J. W., Vincent, R. K., Logan, L. M., and Hunt, G. R.: 1970, *J. Geophys. Res.* **75**, 2671.
Shorthill, R. W., Saari, J. M., Baird, F. E., and LeCompte, J. R.: 1969, 'Photometric Properties of Selected Lunar Features', NASA Contractor Report CR-1429.
Sinton, W. M.: 1962, in *Physics and Astronomy of the Moon* (ed. by Z. Kopal), Chap. 11, Academic Press, New York.
Winter, D. F., Bastin, J. A., and Allen, D. A.: 1972, *Lunar Thermal Characteristics* (ed. by J. W. Lucas), Amer. Inst. Aeronautics and Astronautics Progress Series, AIAA Press (in press).
Winter, D. F. and Krupp, J. A.: 1971, *The Moon* **2**, 279.
Winter, D. F. and Saari, J. M.: 1969, *Astrophys. J.* **156**, 1135.